

Syntheses, Structures and Photocurrent Response Properties of Two Crystals Based on Tetrathiafulvalene Derivatives^①

XIAO Ning^{a, c} HAN Lei^a WEN Yi-Hang^{b②}
WANG Le-Jia^c XIAO Xun-Wen^c

^a (School of Material Science and Chemical Engineering, Ningbo University, Ningbo 315211, China)

^b (Zhejiang Key Laboratory for Reactive Chemistry On Solid Surfaces, Institute of Physical Chemistry, Zhejiang Normal University, Jinhua, Zhejiang 321004, China)

^c (School of Material and Chemical Engineering, Ningbo University of Technology, Ningbo 315211, China)

ABSTRACT In this paper, two compounds $[\text{Zn}_2^{2+}(\text{2,6-bis(4'-pyridyl)-TTF})(\text{TPA})_2]^{2-}$ (**1**) and $[\text{Cd}^{2+}(\text{2,6(7)-bis(4'-pyridyl)-TTF})(\text{TPA})_2(\text{H}_2\text{O})_2]$ (TTF = tetrathiafulvalene, TPA = terephthalic acid) (**2**) were synthesized by using solvothermal method and characterized by single-crystal X-ray. The purity of the two compounds was confirmed by their PXRD data. We also tested the photocurrent responses of these two compounds, and found they could generate photocurrent signal when exposed to light, but the photocurrent intensity of compound **2** is significantly greater than that of **1**. From the crystal structure analysis, the possible reason for this phenomenon is that **2** has a more compact ligand arrangement than **1**, leading to a higher carrier density and easier excitation.

Keywords: 2,6(7)-bis(4'-pyridyl)-tetrathiafulvalene, crystal structure, interpenetrating, photocurrent responses; DOI: 10.14102/j.cnki.0254-5861.2011-3011

1 INTRODUCTION

Metal-organic frameworks (MOFs) are a kind of porous crystalline compounds built from metal-based nodes or clusters connected with organic ligands. Researchers are making many efforts to combine functional organic ligands in MOFs in recent years not only due to their intriguing structural topologies but also to their potential applications in a variety of areas, such as catalysis^[1], magnetism^[2], sensors^[3], gas adsorption^[4], electrochemistry^[5] and so on.

The functional MOFs can be built from metal-based nodes with functional organic ligands. Using the redox-active ligands in MOFs could offer a new stage to get redox-active network, which could be used as fuel cells, electrical switch and super-capacitors. As a result, combined redox-active organic ligand in MOFs is a practicable strategy to construct redox-active MOFs. It is well known that TTF (TTF = tetrathiafulvalene) and its derivatives, as electron-rich molecules, have strong electron-donor ability and have two reversible oxidation valence states. And more, the TTF

molecule could be easily functionalized with coordination unit, such as benzoic and pyridine unit. So, an effective way to synthesize redox MOFs is to use TTF and its derivatives as the organic ligands^[6, 7]. Among the TTF derivatives, the common modified groups are carboxylic groups, such as TTF-tetrabenzoate (H_4TTFB)^[8] and pyridine groups like tetra(4-pyridyl)TTF ($\text{TTF}(\text{py})_4$)^[9]. $\text{Zn}_2(\text{TTFB})$ represents the first example of a permanently porous MOF with high charge mobility. The compound exhibits both columnar stacks of TTF and permanent pores lined by benzoate linkers and the charge mobility is comparable to that of the best conductive organic polymers. Multifunctional metal-organic frameworks have been developed, in which magnetic and electronic can be controlled simultaneously in the same compound. And the conductivity of the material is significantly increased by I_2 doping; the SCO behavior is also modified and the photo-magnetic behavior is turned off. A crystal-to-crystal transformation caused by I_2 doping is also observed. We herein selected 2,6(7)-bis(4'-pyridyl)-TTF ($\text{TTF}(\text{py})_2$)^[10] as a functional ligand to synthesize two novel MOFs compounds.

Received 26 October 2020; accepted 8 December 2020 (CCDC 1847107 for **1** and 1851010 for **2**)

① This work was supported by the Natural Science Foundation of Zhejiang Province (LY18B020016) and Ningbo Science and Technology Innovation 2025(2018B10033)

② Corresponding author. E-mail: wyh@zjnu.edu.cn

We got two new MOFs based on the TTF derivatives, and π - π stacking and multiple interpenetrating structures are found in them. Photoelectric active electrodes of these two compounds were prepared, and their photocurrent properties were studied.

2 EXPERIMENTAL

All reagents and solvents of reagent grade were obtained from commercial channels and used directly without further purification. And the ligand 2,6(7)-bis(4'-pyridyl)-TTF was prepared according to the method reported in the literature^[11]. The PXRD data of compounds **1** and **2** were collected by a Bruker D8 focus X-ray diffractometer with CuK α radiation of wavelength $\lambda = 1.5418 \text{ \AA}$ in the scanning range of 2θ from 5° to 70° at room temperature. CHI660E electrochemical workstation was used to carry out the photocurrent response experiments.

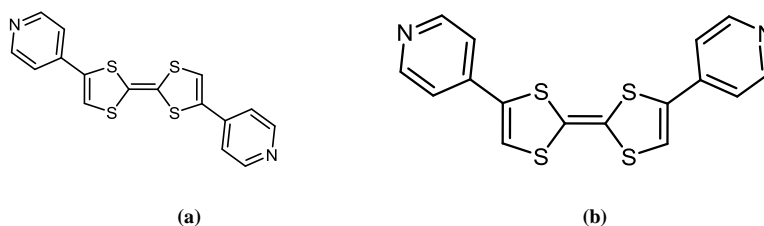
2.1.1 Synthesis of compound 1

The 2,6(7)-bis(4'-pyridyl)-TTF (0.036 g, 0.1 mmol) was dissolved in 20 mL DMF and stirred for 15 min at room

temperature. Then, $\text{Zn}(\text{NO}_3)_2 \cdot 6\text{H}_2\text{O}$ (0.03 g, 0.1 mmol) and terephthalic acid (TPA) (0.017 g, 0.1 mmol) were added to the DMF solution. Finally, 5 mL of water and methanol was added to the solution. The mixed solution was stirred homogeneously for 10 minutes. Then the solution was sealed in a stainless-steel autoclave and heated at 85°C for 3 days. Deep red block crystals of compound **1** were obtained after cooling to room temperature. Crystals were washed and filtered with deionized water and dried at room temperature (Yield: 13.89 mg, 34% based on Zn(II)). Anal. Calcd. (%) for $\text{C}_{32}\text{H}_{18}\text{N}_2\text{O}_8\text{S}_4\text{Zn}_2$: C, 47.02; H, 2.20; N, 3.43. Found (%): C, 46.96; H, 2.24; N, 3.37.

2.1.2 Synthesis of compound 2

Compound **2** was prepared by a similar method to compound **1**. $\text{Cd}(\text{ClO}_4)_2 \cdot 6\text{H}_2\text{O}$ provided cadmium ions. Dark red plate crystals were obtained, followed by washing and filtering with deionized water and drying at room temperature (Yield: 24.83 mg, 36% based on Cd(II)). Anal. Calcd. (%) for $\text{C}_{24}\text{H}_{19}\text{CdN}_2\text{O}_7\text{S}_4$: C, 41.90; H, 1.31; N, 3.49. Found (%): C, 41.87; H, 1.35; N, 3.45.



Scheme 1. Two structures of molecule 2,6(7)-bis(4'-pyridyl)-tetrathiafulvalene

2.2 Structure determination

Suitable single crystal was selected and immobilized on a Bruker APEX-II CCD diffractometer. Data were collected by using a graphite-monochromatic MoK α radiation ($\lambda = 0.71073 \text{ \AA}$) at room temperature. The software of CrysAlisPro Agilent Technologies was used for collecting the frames of data, indexing the reflections, and determining the lattice constants, absorption correction and data reduction^[12]. Using Olex2^[13], the structure was solved by the ShelXT^[14] structure solution program using Intrinsic Phasing and refined by full-matrix least-squares method using the SHELXL^[15] on F^2 . All non-hydrogen atoms were refined anisotropically, and hydrogen

atoms were located using the geometric method. Compound **1** crystallizes in triclinic system, space group $P\bar{1}$ with $a = 10.9220(8)$, $b = 10.9591(9)$, $c = 21.1760(17) \text{ \AA}$, $V = 2480.2(3) \text{ \AA}^3$, $Z = 2$, $\text{C}_{32}\text{H}_{18}\text{N}_2\text{O}_8\text{S}_4\text{Zn}_2$, $M_r = 817.46$, $D_c = 1.095 \text{ g/cm}^3$, $F(000) = 824$, the final $R = 0.0798$ and $wR = 0.2698$ for 11438 observed reflections ($I > 2\sigma(I)$). Compound **2** crystallizes in monoclinic system, space group $P2_1/c$, with $a = 10.4375(4)$, $b = 10.9735(5)$, $c = 11.6833(5) \text{ \AA}$, $V = 1299.92(13) \text{ \AA}^3$, $Z = 2$, $\text{C}_{24}\text{H}_{19}\text{CdN}_2\text{O}_7\text{S}_4$, $M_r = 688.05$, $D_c = 1.758 \text{ g/cm}^3$, $F(000) = 690$, the final $R = 0.0225$ and $wR = 0.0601$ for 2995 observed reflections ($I > 2\sigma(I)$). Selected bond distances and bond angles are listed in Table 1.

Table 1. Selected Bond Lengths (\AA) and Bond Angles ($^\circ$) for **1** and **2**

Compound 1					
Bond	Dist.	Bond	Dist.	Bond	Dist.
Zn(1)–O(1)#1	2.08(3)	Zn(1)–O(3)	2.02(3)	Zn(1)–O(5)	2.03(3)
To be continued					

Zn(1)–O(7)#2	2.05(3)	Zn(1)–N(2)#3	2.04(3)	Zn(2)–O(2)#1	2.06(3)
Zn(2)–O(4)	2.04(3)	Zn(2)–O(6)	2.03(3)	Zn(2)–O(8)#2	2.04(3)
Zn(2)–N(1)	2.04(3)	O(1)–Zn(1)#4	2.08(3)	O(2)–Zn(2)#4	2.06(3)
O(7)–Zn(1)#5	2.05(3)	O(8)–Zn(2)#5	2.04(3)	N(2)–Zn(1)#6	2.04(3)
Angle	(°)	Angle	(°)	Angle	(°)
O(1)#1–Zn(1)–Zn(2)	77.9(10)	O(3)–Zn(1)–Zn(2)	80.5(10)	O(3)–Zn(1)–O(1)#1	158.4(14)
O(3)–Zn(1)–O(5)	91.0(14)	O(3)–Zn(1)–O(7)#2	88.4(2)	O(3)–Zn(1)–N(2)#3	97.2(14)
O(5)–Zn(1)–Zn(2)	82.3(9)	O(5)–Zn(1)–O(1)#1	86.6(13)	O(5)–Zn(1)–O(7)#2	159.5(13)
O(5)–Zn(1)–N(2)#3	100.6(13)	O(7)#2–Zn(1)–Zn(2)	77.3(9)	O(7)#2–Zn(1)–O(1)#1	87.3(13)
N(2)#3–Zn(1)–Zn(2)	176.4(10)	N(2)#3–Zn(1)–O(1)#1	104.3(14)	N(2)#3–Zn(1)–O(7)#2	99.9(13)
O(2)#1–Zn(2)–Zn(1)	81.9(10)	O(4)–Zn(2)–Zn(1)	79.2(10)	O(4)–Zn(2)–O(2)#1	161.1(14)
O(4)–Zn(2)–N(1)	94.5(14)	O(6)–Zn(2)–Zn(1)	77.5(9)	O(6)–Zn(2)–O(2)#1	88.0(13)
O(6)–Zn(2)–O(4)	89.1(14)	O(6)–Zn(2)–O(8)#2	160.0(2)	O(6)–Zn(2)–N(1)	98.5(13)
O(8)#2–Zn(2)–Zn(1)	82.5(9)	O(8)#2–Zn(2)–O(2)#1	89.4(13)	O(8)#2–Zn(2)–O(4)	86.9(14)
O(8)#2–Zn(2)–N(1)	101.4(13)	N(1)–Zn(2)–Zn(1)	172.5(10)	N(1)–Zn(2)–O(2)#1	104.4(14)
C(1)–O(1)–Zn(1)#4	129(3)	C(1)–O(2)–Zn(2)#4	124(3)	C(8)–O(3)–Zn(1)	127(3)
C(8)–O(4)–Zn(2)	128(3)	C(16)–O(5)–Zn(1)	124(3)	C(16)–O(6)–Zn(2)	131(3)
C(9)–O(7)–Zn(1)#5	130(3)	C(9)–O(8)–Zn(2)#5	123(3)	C(17)–N(1)–Zn(2)	121(3)
C(19)–N(1)–Zn(2)	120(3)	C(30)–N(2)–Zn(1)#6	120(3)	C(32)–N(2)–Zn(1)#6	122(3)
Symmetry codes: #1: $x, 1+y, z$; #2: $1+x, y, z$; #3: $x, y, -1+z$; #4: $x, -1+y, z$; #5: $-1+x, y, z$; #6: $x, y, 1+z$					

Compound 2

Bond	Dist.	Bond	Dist.	Bond	Dist.
Cd(1)–N(1)#1	2.2921(16)	Cd(1)–N(1)	2.2921(16)	Cd(1)–O(1)	2.3447(15)
Cd(1)–O(1)#1	2.3447(15)	Cd(1)–O(2)#1	2.3924(15)	Cd(1)–O(2)	2.3924(15)
C(1)–C(1)#2	1.346(4)	C(10)–C(12)#3	1.381(3)	C(12)–C(10)#3	1.381(3)
Angle	(°)	Angle	(°)	Angle	(°)
N(1)#1–Cd(1)–N(1)	112.19(9)	N(1)–Cd(1)–O(1)	98.98(6)	N(1)#1–Cd(1)–O(1)	84.61(6)
N(1)–Cd(1)–O(1)#1	84.61(6)	N(1)#1–Cd(1)–O(1)#1	98.98(6)	N(1)–Cd(1)–O(2)#1	137.79(6)
N(1)#1–Cd(1)–O(2)#1	87.75(6)	N(1)–Cd(1)–(2)	87.75(6)	N(1)#1–Cd(1)–O(2)	137.79(6)
N(1)–(1)–C(9)	91.98(6)	N(1)#1–Cd(1)–C(9)	111.79(6)	N(1)#1–Cd(1)–C(9)#1	91.98(6)
N(1)–Cd(1)–C(9)#1	111.79(6)	O(1)#1–Cd(1)–(1)	173.63(9)	O(1)–Cd(1)–O(2)#1	120.39(6)
O(1)#1–Cd(1)–O(2)#1	54.85(5)	O(1)–Cd(1)–O(2)	54.85(5)	O(1)#1–Cd(1)–O(2)	120.39(6)
O(1)–Cd(1)–C(9)#1	147.85(7)	O(1)–Cd(1)–C(9)	27.49(6)	O(1)#1–Cd(1)–C(9)	147.85(7)
O(1)#1–Cd(1)–C(9)#1	27.49(6)	O(2)–Cd(1)–O(2)#1	102.08(8)	O(2)–Cd(1)–C(9)	27.47(6)
O(2)#1–(1)–C(9)#1	27.47(6)	O(2)–Cd(1)–C(9)#1	115.46(5)	O(2)#1–Cd(1)–C(9)	115.46(5)
C(9)–Cd(1)–C(9)#1	137.34(8)	C(7)–N(1)–Cd(1)	123.87(13)	C(8)–N(1)–Cd(1)	119.73(14)
C(9)–O(1)–Cd(1)	92.80(12)	C(9)–O(2)–Cd(1)	90.64(12)	C(1)#2–C(1)–S(1)	121.76(6)
C(1)#2–C(1)–S(2)	123.56(6)	O(1)–C(9)–Cd(1)	59.71(10)	O(2)–C(9)–Cd(1)	61.89(10)
C(10)–C(9)–Cd(1)	171.37(13)	C(12)#3–C(10)–C(9)	120.57(17)	C(12)#3–C(10)–C(11)	119.14(17)
C(10)#3–C(12)–C(11)	120.57(19)				
Symmetry codes: #1: $2-x, y, 3/2-z$; #2: $1-x, y, 5/2-z$; #3: $1-x, -y, 1-z$					

Table 2. Hydrogen Bond Lengths (Å) and Bond Angles (°) for Compound 2

D–H···A	d(D–H)	d(H···A)	d(D···A)	∠DHA
O(1W)–H(1WA)···O(1)	0.91	2.04	2.812(3)	142
O(1W)–H(1WB)···O(2)#1	1.04	1.82	2.861(3)	177
O(2W)–H(2W)···O(1W)	0.96	1.85	2.799(3)	172
C(3)–H(3)···O(1)#2	0.93	2.63	3.275(3)	127
C(7)–H(7)···O(2W)#3	0.93	2.45	3.247(3)	144

Symmetry codes: #1: $x, -y, -1/2+z$; #2: $x, 1-y, 1/2+z$; #3: $2-x, 1-y, 1-z$

3 RESULTS AND DISCUSSION

3.1 Description of the crystal structures

Structure of compound **1**: X-ray structural analysis indicated that compound **1** crystallizes in triclinic space group $P\bar{1}$. The asymmetric unit contains one TTF(py)₂ molecule, two TPA

anions and two divalent zinc ions. As shown in Fig. 1, the zinc ion is five-coordinated with four carboxylate oxygen atoms on four different TPA anions and one nitrogen atom from the TTF(py)₂ molecule, respectively. The Zn–O bonds are 2.02(3) to 2.08(3) Å, and Zn–N are 2.04(3) Å, all consistent with the previously reported data^[16, 17].

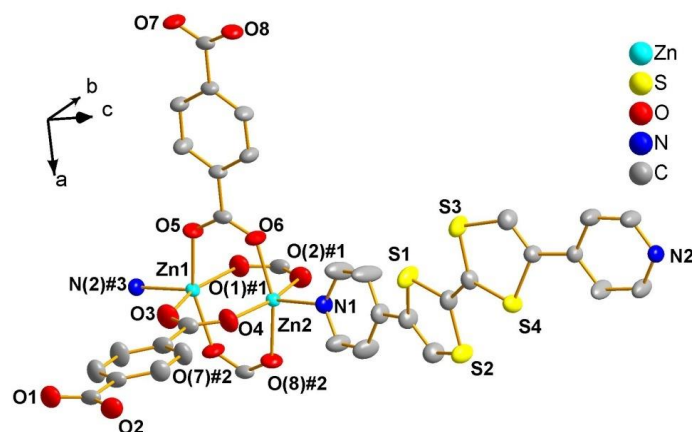


Fig. 1. Coordination environments of Zn(II) in compound **1**. The hydrogen atoms are omitted for clarity (50% ellipsoid probability). Symmetry codes: #1: $x, 1 + y, z$; #2: $1 + x, y, z$; #3: $x, y, -1 + z$

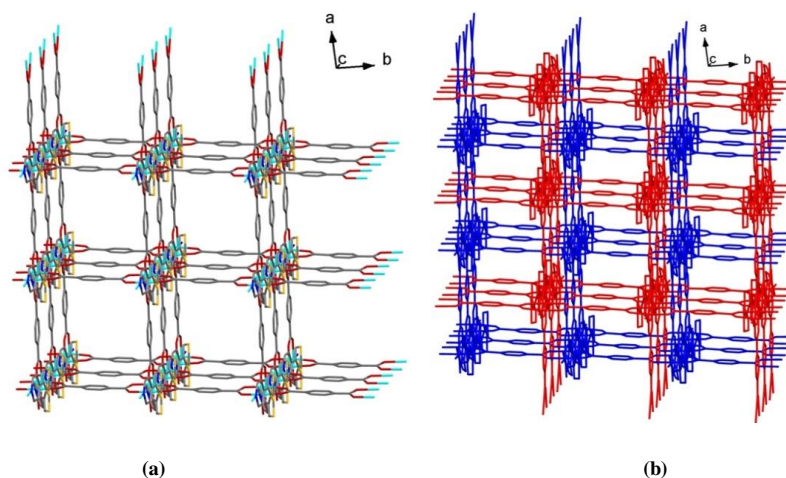


Fig. 2. (a) Haploid 3D frame as seen from the c axis. (b) A double interpenetrating frame structure observed from the c axis

Carboxylic acid group at one end of the TPA anion coordinates with two adjacent zinc ions (Zn(1) and Zn(2)) in the asymmetric unit and takes a monodentate coordination mode. Thus the two adjacent zinc atoms form a binary metal secondary building unit (SBU). On the basis of topological knowledge, the binuclear zinc metal center can be viewed as a node with a simple cubic coordination structure. Four TPA anions are uniformly distributed on a plane that passes through SBU. Herein a two-dimensional network is formed. And two TTF(py)₂ molecules are located in the vertical direction of this 2D network and are connected to another 2D

network via the N–Zn bonds to further form a 3D framework. Further observation revealed that the whole crystal is a 2-fold interpenetrating structure, as shown in Fig. 2. The two interpenetrating 3D frames are fixed by van der Waals forces ($S(2)–O(2) = 3.254(3)$ Å) and π – π stacking interactions (between phenyl rings of TPA anions and the five-membered rings of TTF(py)₂ molecules, centroid-to-centroid distance: $3.600(2)$ Å).

Structure of compound **2**: The change in the position of the pyridine rings of the TTF(py)₂ molecules and the difference in the type of metal ions resulted in a significant change in the

crystal structure. Through single-crystal X-ray diffraction, the crystal structure is growing with space group $P2_1/c$. The asymmetric unit consists of half a $\text{TTF}(\text{py})_2$ molecule, half a TPA anion, one divalent cadmium ion, one water molecule, and one hydroxide anion. One cadmium ion coordinates with

four oxygen atoms and two nitrogen atoms to form a distorted octahedral geometry, as shown in Fig. 3. The Cd–O bond distances are 2.3447(15) to 2.3924(15) Å, and the Cd–N are 2.2921(16) Å, similar to the those in the related cadmium(divalent) compounds^[18, 19].

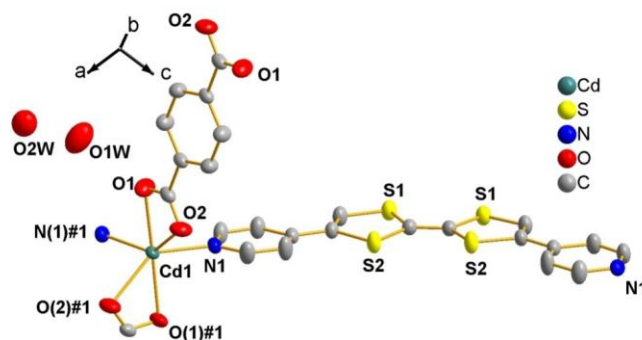


Fig. 3. Coordination environments of Cd(II) in compound 2. The hydrogen atoms are omitted for clarity (50% ellipsoid probability). Symmetry code: #1: $2-x, y, 3/2-z$

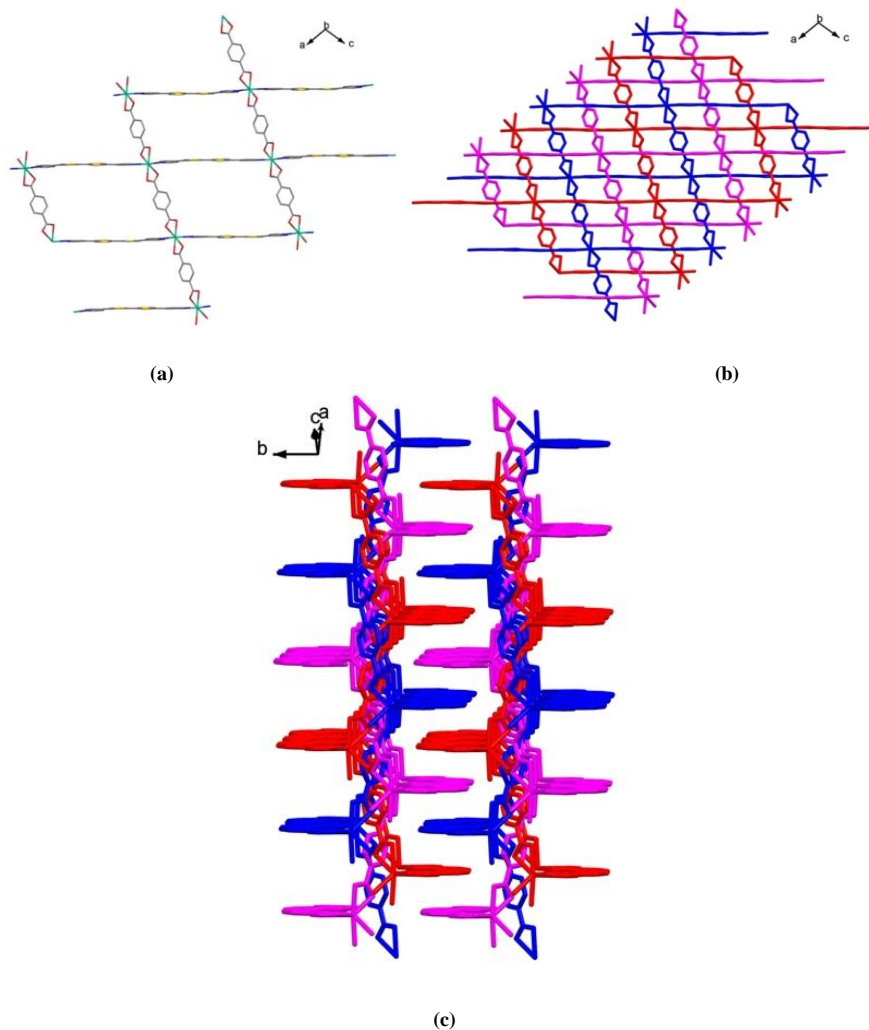


Fig. 4. (a) 2D plane of a single layer observed along the b axis. (b) A 2D plane with a triple penetration observed along the b axis. (c) The plane formed by a triple penetration observed along the $(a-c)$ axis. And the plane continues to pile up along the b axis

Because the carboxylic acid group at one end of the TPA anion adopts a bidentate mode to connect one cadmium ion, a nitrogen atom at one end of the TTF(py)₂ molecule is linked to a cadmium ion. And the two kinds of ligands are not in the same direction. A two-dimensional planar structure is formed (Fig. 4a). The two pyridine rings in the TTF(py)₂ molecule and the two five-membered rings in the TTF core are almost coplanar. And this plane is perpendicular to the two-dimensional network (Fig. 4b). The TTF(py)₂ molecules are arranged on both sides of the two-dimensional network in a staggered way. The two-dimensional networks are further interpenetrated. Unlike the first crystal, it is triple interleaved with a two-dimensional network, resulting in a more compact two-dimensional planar structure (Fig. 4c). The stability of the three planes is dependent on hydrogen bonds between ligands and ligands, ligands and water, and water and water (Table 2). The hydrogen bonds are O(1W)–H(1WA)···O(1) (2.812(3) Å), O(1W)–H(1WB)···O(2)#1 (2.861(3) Å) and O(2W)–H(2W)···O(1W) (2.799(3) Å). A three-dimensional structure is formed by the stacking of the 3-fold interpenetrating planes.

Interestingly, the 3-fold interpenetrating plane (Fig. 4b) has more TTF(py)₂ ligands distributed on both sides. The TTF(py)₂ ligands bite into each other like a zipper when the 3-fold interpenetrating planes are stacked. And the TTF(py)₂ ligands form hydrogen bonds with the 3-fold interpenetrating planes (hydrogen bonds in Table 2). The hydrogen bonds are C(3)–H(3)···O(1)#2 (3.275(3) Å) and C(7)–H(7)···O(2W)#3 (3.247(3) Å). They make the 3-fold interpenetrating planes fixed between each other. The π - π interaction between TTF(py)₂ ligands (distance = 3.653(4) Å) further stabilized the structure.

3. 2 PXRD and photocurrent response properties

3. 2. 1 PXRD analyses

We carried out the PXRD experiment of compounds **1** and **2**, respectively at room temperature. The experimental data of compounds **1** and **2** are fit well with those simulated data from the single crystal, as shown in Fig. 5a and 5b. And more, the main peaks in Fig. 5 are well matched, which may prove the purity phase of these two crystals.

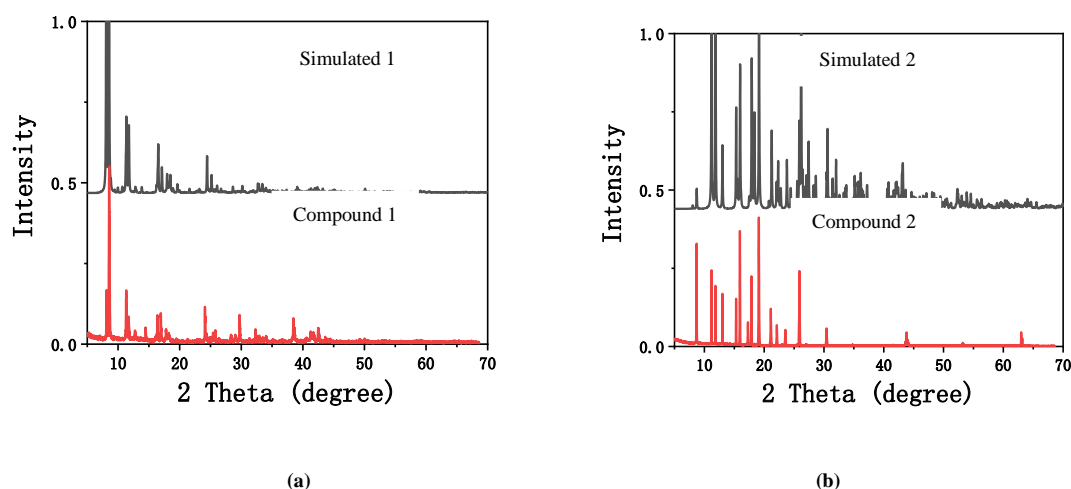


Fig. 5. XRD patterns for the experimental and calculated results of compounds **1** and **2** to ensure their phase purity

3. 2. 2 Photocurrent response properties

Photocurrent response experiments were carried out with CHI660E electrochemical workstation. Compounds **1** and **2** were ground well into powder and then evenly smeared (1.0cm × 1.0cm, 100 Ω/mL) onto ITO glass. ITO conductive glass was used as the working electrode, Pt as the auxiliary electrode, and saturated calomel electrode (SCE) as the reference electrode. 0.1 M Na₂SO₄ solution was used as the supporting electrolyte. The power of high voltage xenon lamp as light source is 150 W. The distance between light source and ITO glass is 20 cm. The test was performed with an initial

voltage of 0.8 V and a 20 s time interval. The experimental data are shown in Fig. 6.

Once irradiated with Xe light, the photocurrent was instantly obtained at the highest value. On the other hand, the photocurrent can be immediately reduced to its initial level when the Xe light was off. The phenomenon can be repeated several times, which indicate that these MOFs are stable enough. However, the photocurrent intensity of **1** and **2** is lower than 1.0 uA due to the hydrogen bonding between the receptor unit bpy or bpy-ete unit and TTF unit. However, the photocurrent was very stable without a decrease in the

intensity, which means HOFs **1** and **2** are stable.

The results showed that compounds **1** and **2** had obvious photocurrent signal and sensitive response. When compounds **1** and **2** were irradiated with Xe light, a highest photocurrent was obtained. Once the light was turned off, the photocurrent could be reduced to its original level. Furthermore, their photocurrent was stable and reproducible, indicating that

MOFs **1** and **2** have good stability. We can see that the photocurrent intensity of compound **2** is almost three times that of **1**. This may be related to the structures of the compounds. Compound **2** has more interpenetration multiples, higher overlap between ligands, and tighter ligand alignment, thus leading to a stronger charge transfer capability.

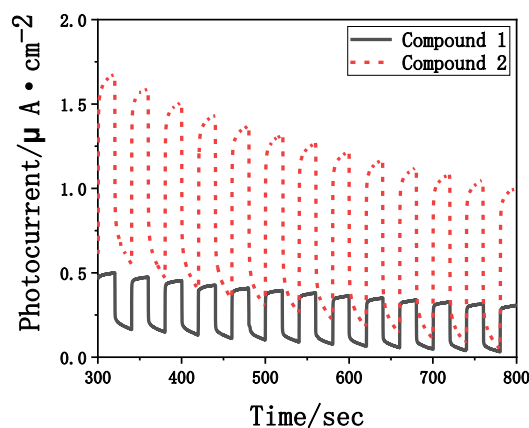


Fig. 6. Photocurrent responses of **1** and **2**

4 CONCLUSION

We have successfully prepared two new Zn(II)/Cd(II) MOFs based on TTF derivatives by hydrothermal synthesis. Crystal data were obtained and analyzed by X-ray diffractometer. The coordination modes of the internal ligands of the crystals were

different due to the change of metal ions and the different configuration of TTF(py)₂. The results of photocurrent based on MOF **1** and **2** were tested, suggesting that the photocurrent intensity was related to the crystal packing. A tighter coordination pattern may be preferable for the photoelectron conversion. As a result, a higher photocurrent is obtained.

REFERENCES

- (1) Roy, S.; Huang, Z.; Bhunia, A.; Castner, A.; Gupta, A. K.; Zou, X.; Ott, S. Electrocatalytic hydrogen evolution from a cobaloxime-based metal-organic framework thin film. *J. Am. Chem. Soc.* **2019**, 141, 15942–15950.
- (2) Ma, X.; Liu, H.; Wen, S.; Xie, Q.; Li, L.; Jin, J.; Wang, X.; Zhao, B.; Song, W. Ultra-sensitive SERS detection, rapid selective adsorption and degradation of cationic dyes on multifunctional magnetic metal-organic framework-based composite. *Nanotechnology* **2020**, 31, 315501–13.
- (3) He, H.; Zhu, Q.; Li, C.; Du, M. Design of a highly-stable pillar-layer zinc(II) porous framework for rapid, reversible, and multi-responsive luminescent sensor in water. *Cryst. Growth Des.* **2019**, 19, 694–703.
- (4) Li, Y.; Zhang, X.; Lan, J.; Xu, P.; Sun, J. Porous Zn(Bmic)(AT) MOF with abundant amino groups and open metal sites for efficient capture and transformation of CO₂. *Inorg. Chem.* **2019**, 58, 13917–13926.
- (5) Gholipour-Ranjbar, H.; Soleimani, M.; Naderi, H. R. Application of Ni/Co-based metal-organic frameworks (MOFs) as an advanced electrode material for supercapacitors. *New J. Chem.* **2016**, 40, 9187–9193.
- (6) Su, J.; Yuan, S.; Wang, T.; Lollar, C. T.; Zuo, J.; Zhang, J.; Zhou, H. Zirconium metal-organic frameworks incorporating tetrathiafulvalene linkers: robust and redox-active matrices for *in situ* confinement of metal nanoparticles. *Chem. Sci.* **2020**, 11, 1918–1925.
- (7) Shen, W.; Xiao, X.; Ye, F.; Wang, M.; Wen, Y. Synthesis, structure and electric property of a 3D supramolecular Co^{II} coordination complex. *Chin. J. Struct. Chem.* **2018**, 37, 1829–1833.
- (8) Narayan, T. C.; Miyakai, T.; Seki, S.; Dincă, M. High charge mobility in a tetrathiafulvalene-based microporous metal-organic framework. *J. Am. Chem. Soc.* **2012**, 134, 12932–12935.

- (9) Wang, H.; Ge, J.; Hua, C.; Jiao, C.; Wu, Y.; Leong, C. F.; D'Alessandro, D. M.; Liu, T.; Zuo, J. Photo- and electronically switchable spin-crossover iron(II) metal-organic frameworks based on a tetrathiafulvalene ligand. *Angew. Chem. Int. Ed.* **2017**, 56, 5465–5470.
- (10) Wang, R.; Kang, L.; Xiong, J.; Dou, X.; Chen, X.; Zou, J.; You, X. Structures and physical properties of oligomeric and polymeric metal complexes based on bis(pyridyl)-substituted TTF ligands and an inorganic analogue. *Dalton Trans.* **2011**, 40, 919–926.
- (11) Han, Y.; Zhang, J.; Lin, Y.; Dai, J.; Jin, G. Synthesis and characterization of half-sandwich iridium complexes containing 2,6(7)-bis(4-pyridyl)-1,4,5,8-tetrathiafulvalene and ancillary ortho-carborane-1,2-dichalcogenolato ligands. *J. Organomet. Chem.* **2007**, 692, 4545–4550.
- (12) *CrysAlisPro*. Rigaku Oxford Diffraction **2015**.
- (13) Dolomanov, O. V.; Bourhis, L. J.; Gildea, R. J.; Howard, J. A. K.; Puschmann, H. OLEX2: a complete structure solution, refinement and analysis program. *J. Appl. Crystallogr.* **2009**, 42, 339–341.
- (14) Sheldrick, G. M. SHELXT-integrated space-group and crystal-structure determination. *Acta Cryst.* **2015**, A71, 3–8.
- (15) Sheldrick, G. M. A short history of SHELX. *Acta Cryst.* **2008**, A64, 112–122.
- (16) Wang, J.; Cao, Z.; Tang, L.; Wang, X.; Hou, X.; Ju, P.; Zhang, E. Two metal ion-controlled Zn(II)/Cd(II) coordination polymers based on 1,3,5-benzenetricarboxylic acid. *Chin. J. Struct. Chem.* **2017**, 10, 1617–1623.
- (17) Li, Z.; Yang, B.; Jiang, Y.; Yu, C.; Zhang, L. Metal-directed assembly of five 4 connected MOFs: one-pot syntheses of MOF-derived MxSy@C composites for photocatalytic degradation and supercapacitors. *Cryst. Growth Des.* **2018**, 18, 979–992.
- (18) Ju, P.; Zhang, E.; Wang, X.; Yang, H.; Wang, J. A novel 3D Cd-based luminescence metal-organic framework: synthesis, structure and luminescent sensing properties. *Chin. J. Struct. Chem.* **2019**, 38, 1578–1584.
- (19) Wang, X.; Li, X.; Pan, Y.; Liu, B.; Zhou, S. A new two-dimensional Cd(II) complex assembled by 1,3,5-benzenetricarboxylic acid and 3-(2-pyridyl)pyrazole. *Chin. J. Struct. Chem.* **2019**, 38, 1275–1282.